Electronic Research Archive

http://www.aimspress.com/journal/era

ERA, 30(8): 3130–3152.
DOI: 10.3934/era.2022159
Received: 04 May 2022
Revised: 31 May 2022
Accepted: 12 June 2022
Published: 16 June 2022

Research article

Numerical simulation of a generalized nonlinear derivative Schrödinger equation

Shasha Bian[1,*], **Yitong Pei**[2,*] **and Boling Guo**[3]

[1] Graduate School of China Academy of Engineering Physics, Beijing 100088, China

[2] Beijing National Laboratory for Condensed Matter Physics, Institute of Physics, Chinese Academy of Sciences, Beijing 100190, China

[3] Institute of Applied Physics and Computational Mathematics, Beijing 100088, China

* **Correspondence:** Email: 1825166115@qq.com, 2584871465@qq.com; Tel: +8618810262679, +8615600917998.

Abstract: In this paper, three nonlinear finite difference schemes are proposed for solving a generalized nonlinear derivative Schrödinger equation which exposits the propagation of ultrashort pulse through optical fiber and has been illustrated to admit exact soliton-solutions. Two of the three schemes are two-level ones and the third scheme is a three-level one. It is proved that the two-level schemes only preserve the total mass or the total energy in the discrete sense and the three-level scheme preserves both the total mass and total energy. Furthermore, many numerical results are presented to test the conservative properties and convergence rates of the proposed schemes. Several dynamical behaviors including solitary-wave collisions and the first-order rogue wave solution are also simulated, which further illustrates the effectiveness of the proposed method for the generalized nonlinear derivative Schrödinger equation.

Keywords: nonlinear derivative Schrödinger equation; finite difference method; conservative properties; simulation of dynamics

1. Introduction

In this paper, we consider a generalized nonlinear derivative Schrödinger (GNLDS) equation [1–3] as follows

$$\begin{aligned} &iu_t + u_{xx} + 2|u|^2u + \gamma_1(u_{xxxx} + 6u_x^2\overline{u} + 4u|u_x|^2 + 8|u|^2u_{xx} \\ &+ 2u^2\overline{u}_{xx} + 6|u|^4u) = 0, \quad x \in [a,b), \quad t \in (0,T], \end{aligned} \tag{1.1}$$

with periodic boundary condition

$$\frac{\partial^m u}{\partial x^m}(a,t) = \frac{\partial^m u}{\partial x^m}(b,t), \quad m = 0,1,2,3, \quad t \in (0,T], \tag{1.2}$$

and initial condition

$$u(x,0) = \varphi(x), \quad x \in [a,b], \tag{1.3}$$

where $u = u(x,t)$ is a complex-valued function, γ_1 denotes the strength of higher-order linear and nonlinear effects, and $\overline{u}$ means taking the conjugate of u.

The GNLDS equation is a integrable system which can be viewed as a particular case of a spin system derived in [1], which advanced the fourth order generalized nonlinear Schrödinger equation for the isotropic Heisenberg ferromagnetic spin chain in the next order of lattice parameter through identifying the underlying geometry of the system, and demonstrated that the spin system with the lattice parameter $\beta = -\frac{5}{2}v$ (v is equivalent to γ_1 in this paper) is equivalent to the higher order integrable generalized nonlinear Schrödinger evolution equation, that is, (1.1). In 2013, Wang, Porsezian and He [2] obtained the first-order rogue wave solution and higher-order rogue waves from the GNLDS evolution equation by using Darboux transformation and Taylor expansion, moreover the compressed effects of parameter γ_1 was talked over. Zhang and Chen [3] studied the robust inverse scattering transformation transformation to construct the high-order rogue wave based on the GNLDS equation in 2019. For the rogue waves and solitary waves, we refer to [4–6] and references therein.

The famous mathematical model nonlinear Schrödinger equation [7, 8] has been widely used in the study of quantum physics and theoretical chemistry, so various highly accurate and effective numerical methods are required and have been developed for the NLS equation, for instance [9–16], finite difference method [17–23], finite element method [24–26], discontinuous Galerkin method [27, 28], meshless method [29, 30], and Runge-Kutta or Crank-Nicolson pseudo-spectral method [31–33], time-splitting pseudo-spectral method [34–38], the spectral and pseudo-spectral method [39–41], split step spectral method [42], structure-preserving algorithms [43–45], and other methods [46–51]. These different numerical methods have their own advantages and disadvantages. For the comparison between them, we refer to [52–54] and references therein. Although above numerical methods have been researched for NLS, as far as we know, there are no corresponding literatures which focused on aspects of numerical simulation of (1.1). Thus, to construct respectively numerical methods is our main work in this paper.

After simple observation and analysis of the equation, we find that

$$\begin{aligned} &6u_x^2\overline{u} + 4u|u_x|^2 + 8|u|^2u_{xx} + 2u^2\overline{u}_{xx} \\ =&6(u_x^2 + uu_{xx})\overline{u} + 2(u_{xx}\overline{u} + 2u_x\overline{u}_x + u\overline{u}_{xx})u \\ =&3(u^2)_{xx}\overline{u} + 2(u\overline{u})_{xx}u, \end{aligned} \tag{1.4}$$

so we simplify the Eq (1.1), then the original question becomes

$$iu_t + u_{xx} + 2|u|^2u + \gamma_1(u_{xxxx} + 3(u^2)_{xx}\overline{u} + 2(u\overline{u})_{xx}u + 6|u|^4u) = 0, \quad x \in [a,b), \ \ t \in (0,T], \tag{1.5}$$

$$u(x,0) = \varphi(x), \quad x \in [a,b], \tag{1.6}$$

$$\frac{\partial^m u}{\partial x^m}(a,t) = \frac{\partial^m u}{\partial x^m}(b,t), \quad m = 0,1,2,3, \quad t \in (0,T]. \tag{1.7}$$

Lemma 1.1. *The initial-boundary value problem* (1.5)–(1.7) *preserves the total mass*

$$\mathrm{Q}(t) := \frac{1}{2}\int_a^b |u|^2 dx \equiv \mathrm{Q}(0), \quad t > 0, \tag{1.8}$$

and energy

$$\begin{aligned}\mathrm{E}(t) := &-\frac{1}{2}\int_a^b |u_x|^2 dx + \frac{1}{2}\int_a^b |u|^4 dx + \frac{\gamma_1}{2}\int_a^b |u_{xx}|^2 dx \\ &- 3\gamma_1 \int_a^b |u_x|^2|u|^2 dx - \frac{\gamma_1}{2}((|u|^2)_x)^2 dx + \gamma_1 \int_a^b |u|^6 dx \equiv \mathrm{E}(0), \quad t > 0.\end{aligned} \tag{1.9}$$

Remark 1.1. Q(t) *and* E(t) *are the so-called mass (or charge) and energy, the process of certification is in* Appendix A.

Hence, to construct an accurate and stable numerical method preserving the total mass and energy is an interesting and challenging issue. However, it is difficult and challenging for us to construct a finite difference scheme which preserves the total mass and energy because of the higher order linear terms and some higher order nonlinear terms with derivatives. For this reason, we first propose two nonlinear two-level schemes, one is mass-preserving and the other is energy-preserving. In further study, we finally construct a three-level mass-preserving and energy-preserving scheme, the three schemes will be shown in the second part. Therefore, it is an exciting problem to explore what will happen to simulate the first-order rogue wave solution and other physical phenomena through our numerical simulation. It is our prime purpose to reply this question in this paper.

The remaining sections of this paper are arranged as follows. Finite difference schemes are constructed and the corresponding discrete conservation laws are proposed in Section 2; Section 3 is devoted to showing the conclusion of our numerical experiments which illustrate the effectiveness of the proposed methods; Finally, Section 4 contains the conclusion of this paper and the researches that need to be progressed in the future.

2. Finite difference schemes and their conservative properties

In order to solve the problem (1.5)–(1.7) with the difference scheme, the solution area $\Omega = \{(x,t)|a \le x \le b, 0 \le t \le \mathrm{T}\}$ will be divided. Take two positive integers N and J, let $h = \frac{(b-a)}{J}, \tau = \frac{T}{N}$, and denote $\Omega_h = \{x_j = a + jh | j = 0, 1, ...J\}$, $\Omega_\tau = \{t_n = n\tau | n = 0, 1, ...N\}$.

Assuming that $\omega = \{\omega_j^n | (x_j, t_n) \in \Omega_h \times \Omega_\tau\}$ is a grid function. We introduce the following standard difference operators:

$$\omega_j^{n+\frac{1}{2}} = \frac{\omega_j^{n+1} + \omega_j^n}{2}, \quad \delta_t^+ \omega_j^n = \frac{\omega_j^{n+1} - \omega_j^n}{\tau}, \quad \delta_x^+ \omega_j^n = \frac{\omega_{j+1}^n - \omega_j^n}{h},$$
$$\delta_x^2 \omega_j^n = \frac{\omega_{j-1}^n - 2\omega_j^n + \omega_{j+1}^n}{h^2}, \quad \delta_{\hat{t}} \omega_j^n = \frac{\omega_j^{n+1} - \omega_j^{n-1}}{2\tau}.$$

We denote by $\mathbb{V}_h = \{v | v = (v_0, v_1, ..., v_J), v_0 = v_J\}$ a space of complex-valued grid functions defined on Ω_h, we always use $v_{-1}^n = v_{J-1}^n$ and $v_1^n = v_{J+1}^n$ if they are involved. For any complex-valued grid

functions $u, v \in \mathbb{V}_h$, we denote the discrete inner product as $(u, v) = h\sum_{j=0}^{J-1} u_j\overline{v}_j$, where $\overline{v}_j$ is the conjugate of v_j. The discrete L_p norm $\|\cdot\|_p$, the H^1 semi-norm $|\cdot|_1$, the H^2 semi-norm $|\cdot|_2$ and the maximum norm $\|\cdot\|_\infty$ over $\mathbb{V}_h$ are defined by

$$\|v\|_p = \sqrt[p]{h\sum_{j=0}^{J-1}|v_j|^p}, \quad |v|_1 = \sqrt{h\sum_{j=0}^{J-1}|\delta_x^+ v_j|^2}, \quad |v|_2 = \sqrt{h\sum_{j=0}^{J-1}|\delta_x^2 v_j|^2}, \quad \|v\|_\infty = \max_{0\le j\le J-1}|v_j|,$$

respectively. For simplicity, we use $\|v\|$ to denote $\|v\|_2$.

2.1. The three Crank-Nicolson-type finite difference schemes

In this section, we present three Crank-Nicolson-type finite difference schemes. Two of them are the two-level mass-preserving scheme or the two-level energy-preserving scheme and the third is a three-level mass-preserving and energy-preserving scheme. We denote the three schemes by CNFD-A, CNFD-B and CNFD-C as follows:

CNFD – A

$$\begin{aligned}
&i\delta_t^+ u_j^n + \delta_x^2 u_j^{n+\frac{1}{2}} + 2|u_j^{n+\frac{1}{2}}|^2 u_j^{n+\frac{1}{2}} + \gamma_1[\delta_x^2\delta_x^2 u_j^{n+\frac{1}{2}} + 3\delta_x^2((u_j^{n+\frac{1}{2}})^2\overline{u}_j^{n+\frac{1}{2}}\\
&+ 2\delta_x^2(u_j^{n+\frac{1}{2}}\overline{u}_j^{n+\frac{1}{2}})u_j^{n+\frac{1}{2}} + 6|u_j^{n+\frac{1}{2}}|^4 u_j^{n+\frac{1}{2}}] = 0, \quad 0 \le j \le J-1, \ \ 0 \le n \le N-1, \qquad (2.1)\\
&u_j^0 = \varphi(x_j), \quad 0 \le j \le J, \qquad (2.2)\\
&u_{0-m}^n = u_{J-m}^n, \quad m = 0, 1, 2, 3, \quad 0 \le n \le N. \qquad (2.3)
\end{aligned}$$

CNFD – B

$$\begin{aligned}
&i\delta_t^+ u_j^n + \delta_x^2 u_j^{n+\frac{1}{2}} + (|u_j^n|^2 + |u_j^{n+1}|^2)u_j^{n+\frac{1}{2}} + \gamma_1[\delta_x^2\delta_x^2 u_j^{n+\frac{1}{2}} + \frac{3}{2}\delta_x^2((u_j^{n+1})^2 + (u_j^n)^2)\overline{u}_j^{n+\frac{1}{2}}\\
&+ \delta_x^2(|u_j^n|^2 + |u_j^{n+1}|^2)u_j^{n+\frac{1}{2}} + 2(|u_j^n|^4 + |u_j^n|^2|u_j^{n+1}|^2 + |u_j^{n+1}|^4)u_j^{n+\frac{1}{2}}] = 0, \qquad (2.4)\\
&0 \le j \le J-1, \quad 0 \le n \le N-1,\\
&u_j^0 = \varphi(x_j), \quad 0 \le j \le J, \qquad (2.5)\\
&u_{0-m}^n = u_{J-m}^n, \quad m = 0, 1, 2, 3, \quad 0 \le n \le N. \qquad (2.6)
\end{aligned}$$

CNFD – C

$$\begin{aligned}
&i\delta_{\hat{t}} u_j^n + \frac{1}{2}\delta_x^2(u_j^{n+1} + u_j^{n-1}) + |u_j^n|^2(u_j^{n+1} + u_j^{n-1}) + \gamma_1[\frac{1}{2}\delta_x^2\delta_x^2(u_j^{n+1} + u_j^{n-1})\\
&+ \frac{3}{2}\delta_x^2(u_j^n(u_j^{n+1} + u_j^{n-1}))\overline{u}_j^n + \frac{1}{2}\delta_x^2(|u_j^{n+1}|^2 + |u_j^{n-1}|^2)(u_j^{n+1} + u_j^{n-1})\\
&+ (|u_j^{n+1}|^4 + |u_j^{n+1}|^2|u_j^{n-1}|^2 + |u_j^{n-1}|^4)(u_j^{n+1} + u_j^{n-1})] = 0, \qquad (2.7)\\
&0 \le j \le J-1, \quad 1 \le n \le N-1,\\
&u_j^0 = \varphi(x_j), \quad 0 \le j \le J, \qquad (2.8)\\
&u_{0-m}^n = u_{J-m}^n, \quad m = 0, 1, 2, 3, \quad 0 \le n \le N. \qquad (2.9)
\end{aligned}$$

2.2. Conservative properties

Corresponding to the conservation laws (1.8) and (1.9) preserved by the continuous problem (1.5)–(1.7), the scheme CNFD-C conserves the similar total mass and energy in the discrete level, the scheme CNFD-B conserves the corresponding total energy in the discrete level, the scheme CNFD-A conserves the corresponding total mass in the discrete level.

Theorem 2.1. *Suppose* $\{u_j^n|0 \le j \le J, 0 \le n \le N\}$ *is the solution of CNFD-A scheme, then CNFD-A scheme has a conservation law of the following form with respect to discrete mass:*

$$\mathrm{Q}^n \equiv \mathrm{Q}^0, \quad 0 \le n \le N, \tag{2.10}$$

where

$$\mathrm{Q}^n := \frac{1}{2}\|u^n\|^2. \tag{2.11}$$

Theorem 2.2. *Suppose* $\{u_j^n|0 \le j \le J, 0 \le n \le N\}$ *is the solution of CNFD-B scheme, then CNFD-B scheme has a conservation law of the following form with respect to discrete energy:*

$$\mathrm{E}^n \equiv \mathrm{E}^0, \quad 0 \le n \le N, \tag{2.12}$$

where

$$\mathrm{E}^n := -\frac{1}{2}|u^n|_1^2 + \frac{1}{2}\|u^n\|_4^4 + \frac{\gamma_1}{2}|u^n|_2^2 - \frac{3h\gamma_1}{4}\sum_{j=0}^{J-1}\delta_x^+(u_j^n)^2\delta_x^+(\overline{u}_j^n)^2 - \frac{h\gamma_1}{2}\sum_{j=0}^{J-1}(\delta_x^+|u_j^n|^2)^2 + \gamma_1\|u^n\|_6^6. \tag{2.13}$$

Theorem 2.3. *Suppose* $\{u_j^n|0 \le j \le J, 0 \le n \le N\}$ *is the solution of CNFD-C scheme, then CNFD-C scheme has conservation laws of the following forms with respect to discrete mass and discrete energy:*

$$\mathrm{Q}^n \equiv \mathrm{Q}^0, \quad 0 \le n \le N-1, \tag{2.14}$$

$$\mathrm{E}^n \equiv \mathrm{E}^0, \quad 0 \le n \le N-1, \tag{2.15}$$

where

$$\mathrm{Q}^n := \frac{1}{2}(\|u^{n+1}\|^2 + \|u^n\|^2), \tag{2.16}$$

$$\begin{aligned}\mathrm{E}^n :=& -\frac{1}{4}(|u^{n+1}|_1^2 + |u^n|_1^2) + \frac{1}{2}\|u^{n+1}u^n\|^2 + \frac{\gamma_1}{4}(|u^{n+1}|_2^2 + |u^n|_2^2) \\ &- \frac{3\gamma_1}{4}|u^{n+1}u^n|_1^2 - \frac{h\gamma_1}{4}\Big(\sum_{j=0}^{J-1}(\delta_x^+|u_j^{n+1}|^2)^2 + \sum_{j=0}^{J-1}(\delta_x^+|u_j^n|^2)^2\Big) + \frac{\gamma_1}{2}(\|u^{n+1}\|_6^6 + \|u^n\|_6^6).\end{aligned} \tag{2.17}$$

Remark 2.1. *Q^n and E^n are the so-called discrete mass (or charge) and energy respectively. The proofs of the three theorems are given in* Appendix B.

3. Numerical examples

In this section, we construct several typical numerical examples to verify conservation laws and convergence rates, and simulate some phenomena of the solitary-wave collisions and the first-order rogue wave solution described by GNLDS equation.

Example 3.1. *Mass and energy conservations laws*: We give several numerical results out to validate the mass and energy conservations of the three schemes given in Theorems 2.1–2.3. Specifically, we take the initial condition and boundary condition as $\varphi(x) = \text{sech(x)exp(2ix)}$, the periodic boundary condition $\frac{\partial^m u}{\partial x^m}(a,t) = \frac{\partial^m u}{\partial x^m}(b,t)$, $m = 0,1,2,3$, and we consider the case $\gamma_1 = 0.5$. Figures 1–4 reveal the development of the mass and energy values of the corresponding numerical solutions for the three schemes. We can observe that, for CNFD-A scheme and CNFD-B scheme

$$\frac{\mathrm{Q}^{\mathrm{n}} - \mathrm{Q}^0}{\mathrm{Q}^0} = O(10^{-13}), \quad \frac{\mathrm{E}^{\mathrm{n}} - \mathrm{E}^0}{\mathrm{E}^0} = O(10^{-13}), \quad 1 \le n \le N, \tag{3.1}$$

for CNFD-C scheme,

$$\frac{\mathrm{Q}^{\mathrm{n}} - \mathrm{Q}^0}{\mathrm{Q}^0} = O(10^{-14}), \quad \frac{\mathrm{E}^{\mathrm{n}} - \mathrm{E}^0}{\mathrm{E}^0} = O(10^{-13}), \quad 1 \le n \le N-1, \tag{3.2}$$

which illustrates that the CNFD-A scheme preserves total mass conservation, the CNFD-B scheme preserves total energy conservation, and the CNFD-C scheme preserves both total energy and mass conservation in discrete sense.

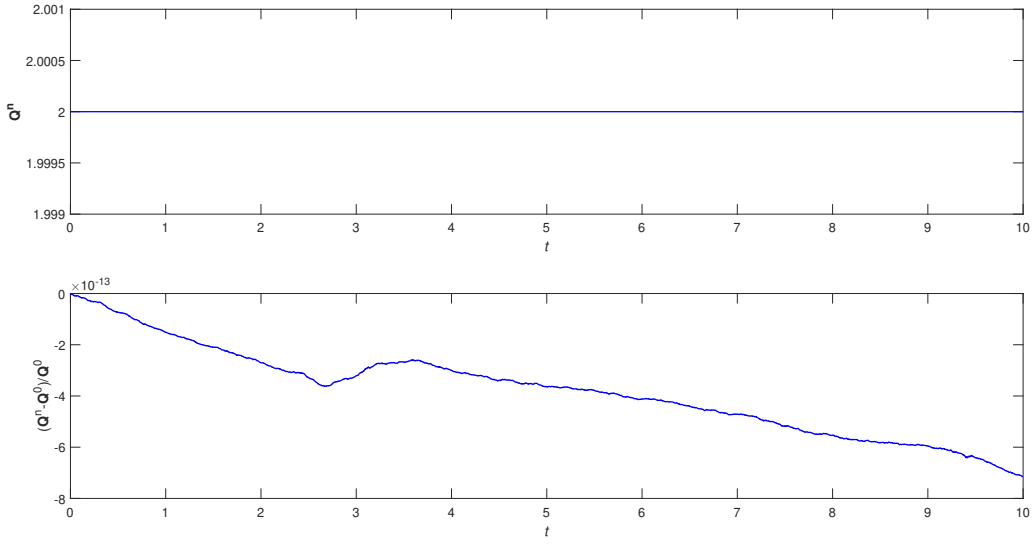

Figure 1. Discrete mass computed by CNFD-A.

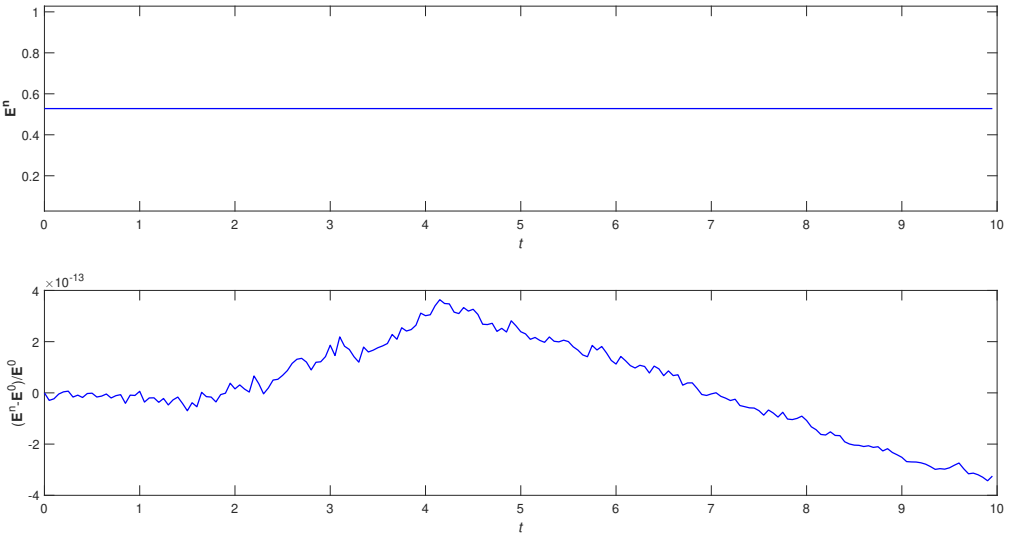

Figure 2. Discrete energy computed by CNFD-B.

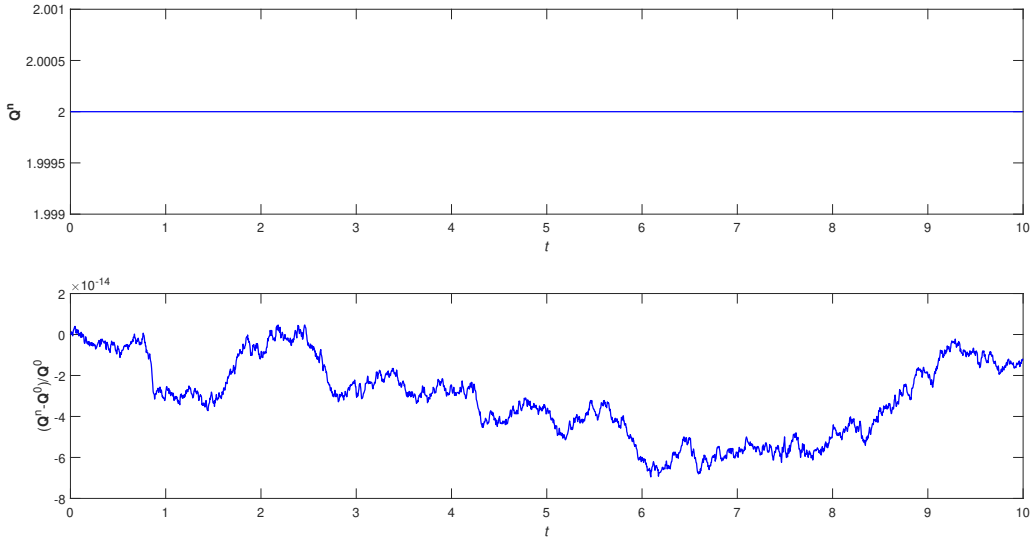

Figure 3. Discrete mass computed by CNFD-C.

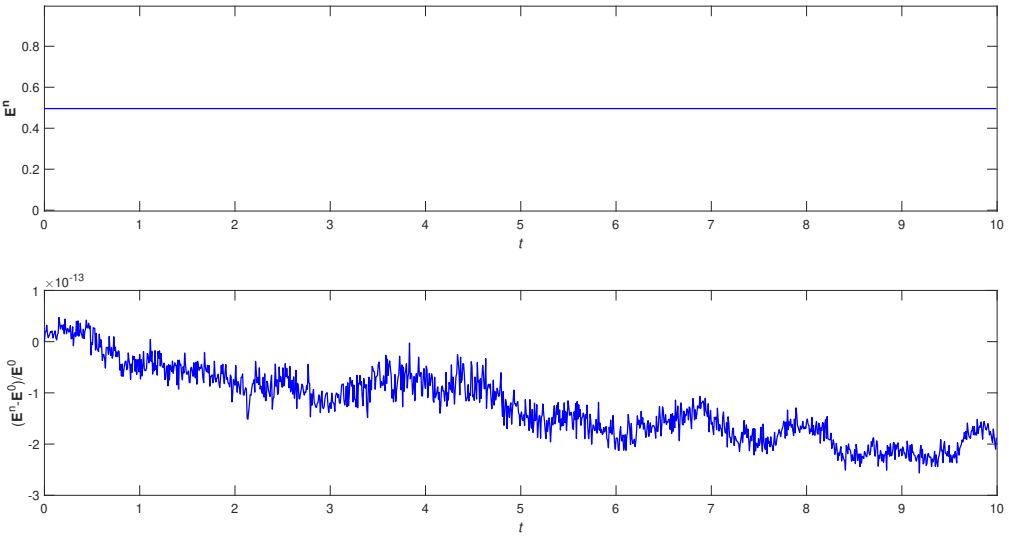

Figure 4. Discrete energy computed by CNFD-C.

Example 3.2. *Convergence rates*: In this example, we take the initial condition and the periodic boundary condition as $\varphi(x) = \text{sech(x)exp(2ix)}$, $\frac{\partial^m u}{\partial x^m}(a,t) = \frac{\partial^m u}{\partial x^m}(b,t)$, $m = 0, 1, 2, 3$ to verify the convergence rates. We consider the case $\gamma_1 = 0.5$, then we compute the L_∞ and L_2 error norms of the solution at $T = 1$ and use the same spacing h in each spatial direction. For convenience, we denote the L_∞ and L_2 error norms as

$$E_\infty(h,\tau) = \|e^n\|_\infty = \max_{1\le j\le J-1} |e_j^n|, \quad E_2(h,\tau) = \|e^n\| = \sqrt{\sum_{j=1}^{J-1} |e_j^n|^2}, \tag{3.3}$$

and assume $E_\infty(h,\tau) = O(\tau^p + h^q)$, then if τ is small enough, $E_\infty(h,\tau) = O(\tau^p + h^q) \approx O(h^q)$, so $E_\infty(h_1,\tau)/E_\infty(h_2,\tau) \approx (h_1/h_2)^q$, and hence $q \approx \frac{\ln(E_\infty(h_1,\tau)/E_\infty(h_2,\tau))}{\ln(h_1/h_2)}$ is the convergence order with respect to the spatial step size. Likewise, if h is small enough, $p \approx \frac{\ln(E_\infty(h,\tau_1)/E_\infty(h,\tau_2))}{\ln(\tau_1/\tau_2)}$ is the convergence order with respect to the temporal step size. The algorithm of L_2 error norm is consistent with L_∞ error norm.

Firstly, we measure the temporal errors and convergence orders. Fix the spatial step size $h = 0.005$ sufficiently small such that the spatial error is negligible as compared with the temporal error. Tables 1, 3 and 5 show that the convergence order of the three schemes with respect to temporal variable are all about 2 when $h = 0.005$, $\tau = 1/70$, $\tau = 1/80$, $\tau = 1/90$, and $\tau = 1/100$.

Through varying h and fixing $\tau = 1/8000$ small enough to avoid contamination of the temporal, we further measure the spatial errors and convergence orders. It can be seen from Tables 2, 4 and 6 show that the convergence order of three schemes are all about 2 with respect to the spatial step size.

Table 1. Rates of temporal convergence for CNFD-A.

τ	E_∞	order	E_2	order
1/70	7.61E-01	—	1.12E-01	—
1/80	5.85E-02	1.97	8.58E-02	1.97
1/90	4.63E-02	1.98	6.79E-02	1.98
1/100	3.76E-02	1.98	5.51E-02	1.98

Table 2. Rates of spatial convergence orders for CNFD-A.

h	E_∞	order	E_2	order
1/10	1.46E-01	—	2.09E-01	—
2/25	9.38E-02	1.99	1.34E-01	1.99
1/20	3.65E-02	2.01	5.22E-02	2.01
1/25	2.33E-02	2.02	3.33E-02	2.02

Table 3. Rates of temporal convergence for CNFD-B.

τ	E_∞	order	E_2	order
1/70	9.83E-02	—	1.40E-01	—
1/80	7.60E-02	1.93	1.08E-01	1.93
1/90	6.05E-02	1.94	8.58E-02	1.95
1/100	4.92E-02	1.95	6.99E-02	1.95

Table 4. Rates of spatial convergence orders for CNFD-B.

h	E_∞	order	E_2	order
1/5	5.63E-01	—	8.10E-01	—
1/10	1.46E-01	1.95	2.09E-01	1.95
2/25	9.38E-02	1.99	1.34E-01	1.99
1/20	3.65E-02	2.01	5.22E-02	2.01

Table 5. Rates of temporal convergence for CNFD-C.

τ	E_∞	order	E_2	order
1/70	1.46E-02	—	2.33E-02	—
1/80	1.13E-02	1.87	1.82E-02	1.86
1/90	9.05E-03	1.92	1.45E-02	1.90
1/100	7.39E-03	1.92	1.19E-02	1.93

Table 6. Rates of spatial convergence orders for CNFD-C.

h	E_∞	order	E_2	order
1/5	5.63E-01	—	8.10E-01	—
2/15	2.58E-01	1.93	3.70E-01	1.93
1/15	6.84E-02	1.92	9.32E-02	1.99
1/20	3.65E-02	2.18	5.22E-02	2.01

Example 3.3. *The influence of γ_1 on the motion of two solitary waves*: In this section, we apply CNFD-C scheme to research the interaction between two solitary waves through changing the value of γ_1. The initial condition is chosen as

$$\varphi(x) = \text{sech(x} - 10)\text{exp(2ix} - 10) + \text{sech(x} + 10)\text{exp(2ix} + 10), \tag{3.4}$$

which illustrates two solitary waves are initially located at $x = 10$ and $x = -10$ and the periodic boundary condition $\frac{\partial^m u}{\partial x^m}(a,t) = \frac{\partial^m u}{\partial x^m}(b,t)$, $m = 0, 1, 2, 3$. We consider the following cases:

$$(1)\quad \gamma_1 = -0.5, \quad (2)\quad \gamma_1 = 0, \quad (3)\quad \gamma_1 = 0.5, \quad (4)\quad \gamma_1 = 1. \tag{3.5}$$

Figures 5 and 6 display the interaction of two solitary waves under different values of γ_1 for GNLDS equation under cases (1)–(4). It can be vividly seen that two initially well-separated solitons move towards each only on the cases $\gamma_1 > 0$, with the motion of the waves, they will produce a peak when they collide, after separation, they will continue to move in the original direction. When $\gamma_1 \leq 0$, compared with $\gamma_1 > 0$, the two solitons move in the opposite direction at the beginning and there are no collisions. In addition, we find that the velocity of the waves is proportional to the absolute value of γ_1.

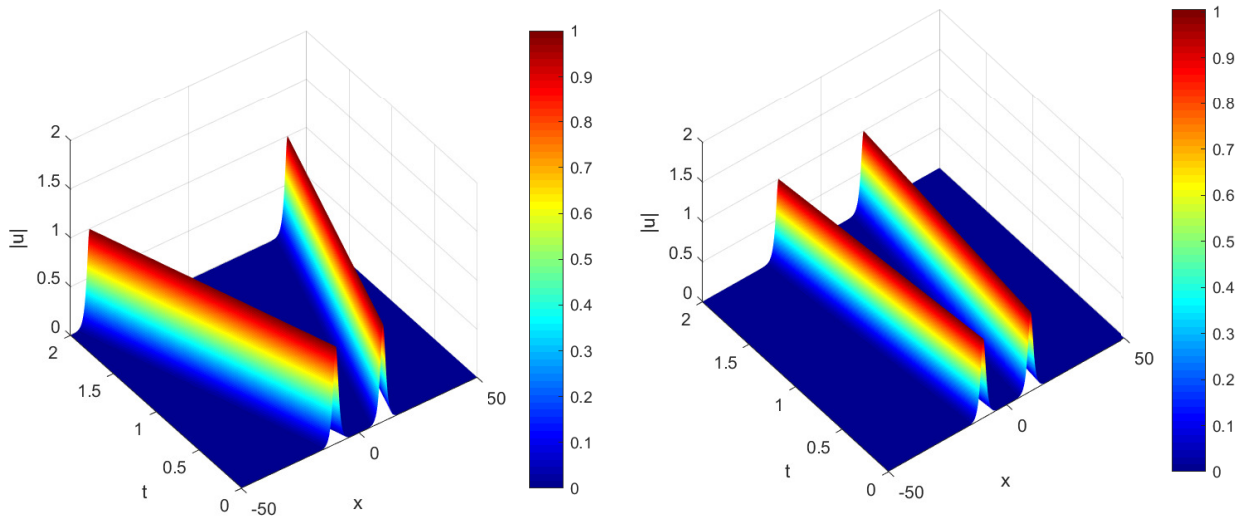

Figure 5. Simulation results of the two solitons computed by CNFD-C under case (1)–(2), Figure (a) presents $\gamma_1 = -0.5$ and Figure (b) presents $\gamma_1 = 0$.

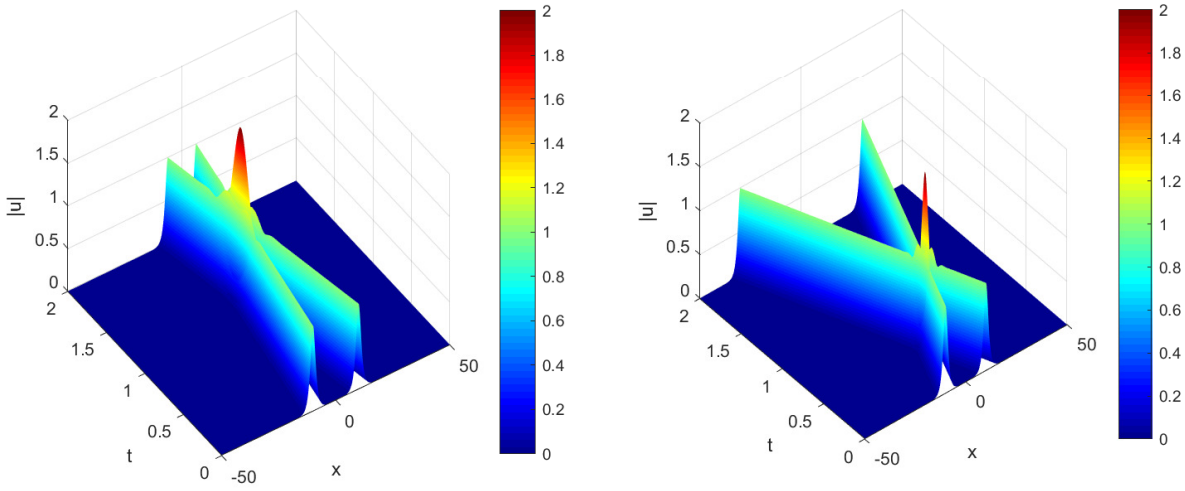

(a) (b)

Figure 6. Simulation of the interaction for the two solitons computed by CNFD-C under case (3)–(4), Figure (a) presents $\gamma_1 = 0.5$ and Figure (b) presents $\gamma_1 = 1$.

Example 3.4. *The first-order rogue wave*: We apply the numerical solution obtained by the CNFD-C scheme to simulate the first-order rogue wave (the limit of the breather solution) [2] in $\{(x,t) \in (a,b)\times(0,T)| -8 \le x \le 8, -4 \le t \le 4\}$. And we also increase the value of γ_1 to observe and compare the dynamical evolution of the analytic solutions and the numerical solutions. We take the initial value of the analytic solution by

$$\varphi(x) = \frac{-x^2+3}{2x^2+2}, \tag{3.6}$$

take the periodic boundary values of the analytic solution by

$$u(a,t) = u(b,t) = \frac{1}{2}\left(\frac{4+i(4+6\gamma_1)t}{64+(1+\frac{3}{2}\gamma_1)^2t^2+1} - 1\right)\exp\left(i\left(\frac{3}{8}\gamma_1+\frac{1}{2}\right)t\right), \tag{3.7}$$

$$u_{xx}(a,t) = u_{xx}(b,t) = \frac{(4+i(4+6\gamma_1)t)(192-(1+\frac{3}{2}\gamma_1)^2t^2-1)}{(64+(1+\frac{3}{2}\gamma_1)^2t^2+1)^3}\exp\left(i\left(\frac{3}{8}\gamma_1+\frac{1}{2}\right)t\right), \tag{3.8}$$

and consider the following cases:

$$(1)\quad \gamma_1 = -1, \quad (2)\quad \gamma_1 = -0.5, \quad (3)\quad \gamma_1 = 0, \quad (4)\quad \gamma_1 = 0.5, \quad (5)\quad \gamma_1 = 1.$$

We show Figures 7–16 as follows, it can be seen that the numerical solutions agree well with the analytic solutions and they have approximately equal amplitudes under cases (1)–(5) which illustrates the effectiveness of CNFD-C.

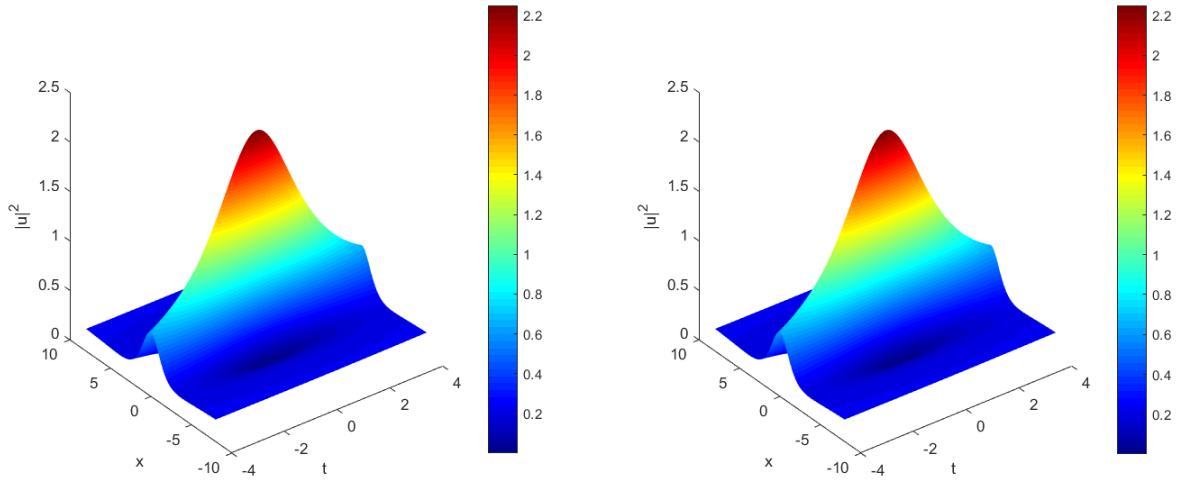

Figure 7. Comparison of dynamics evolution between the analytic solution (left) and the numerical solution (right) for the first-order rogue wave solution under case (1) $\gamma_1 = -1$.

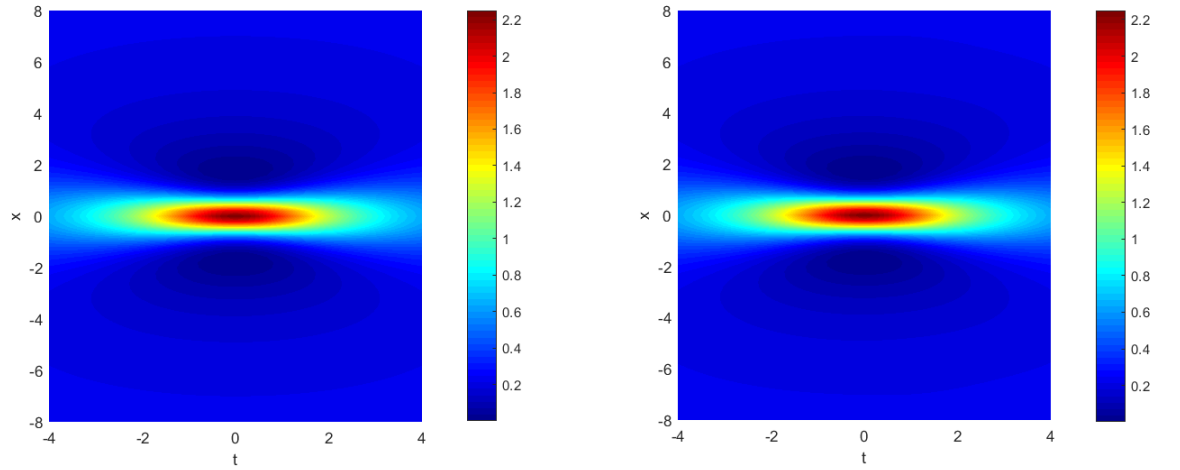

Figure 8. The planform between the analytic solution (left) and the numerical solution (right) of the first-order rogue wave solution under case (1) $\gamma_1 = -1$.

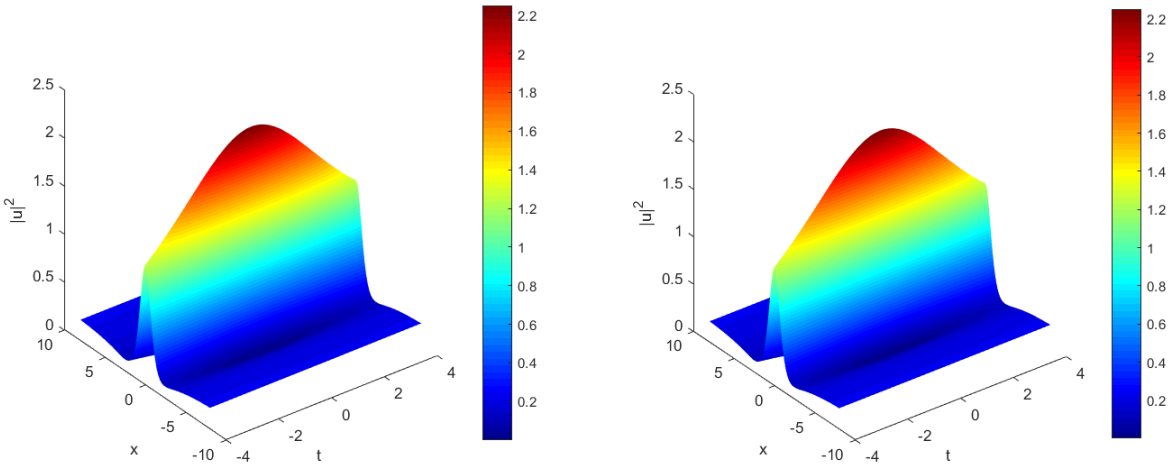

Figure 9. Comparison of dynamics evolution between the analytic solution (left) and the numerical solution (right) for the first-order rogue wave solution under case (2) $\gamma_1 = -0.5$.

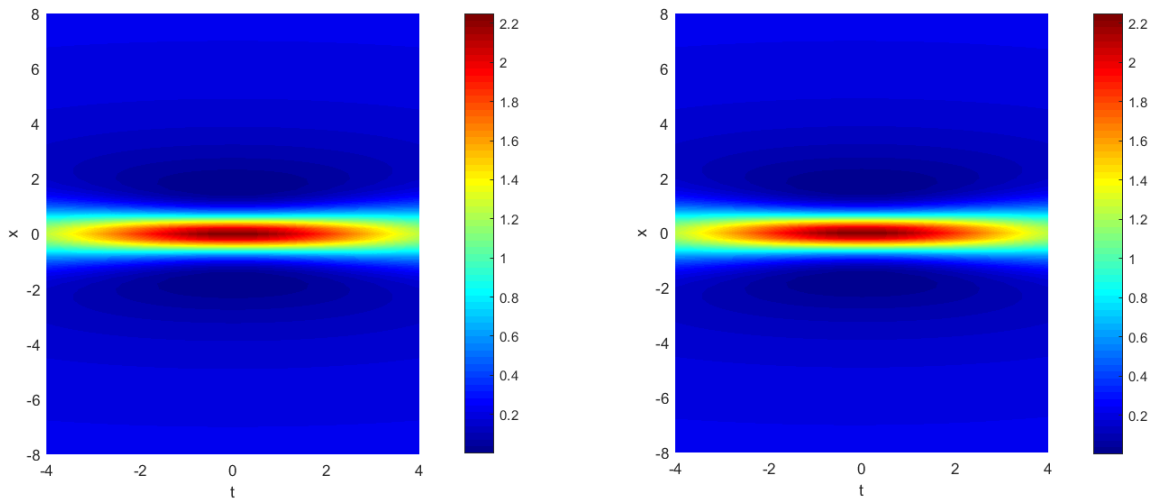

Figure 10. The planform between the analytic solution (left) and the numerical solution (right) of the first-order rogue wave solution under case (2) $\gamma_1 = -0.5$.

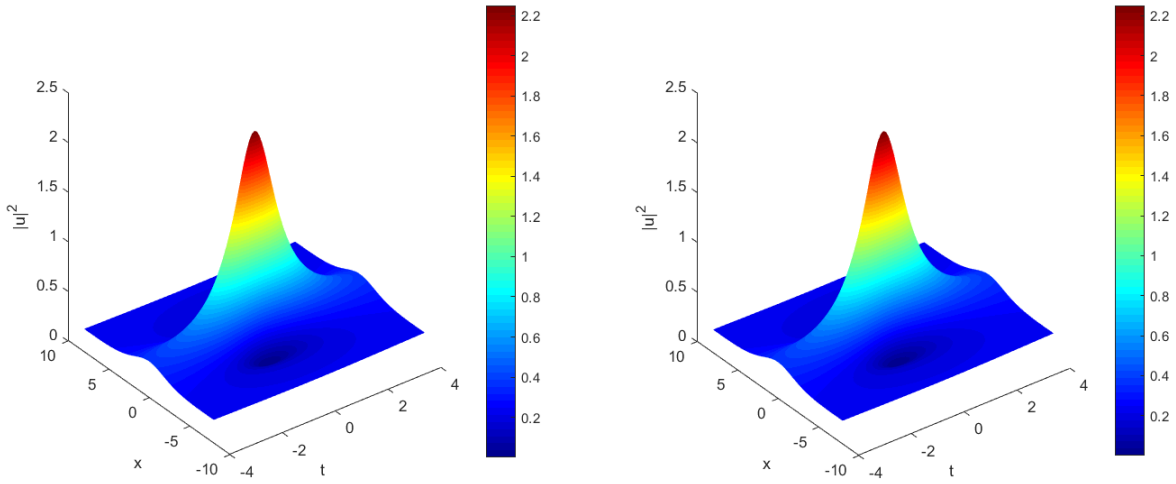

Figure 11. Comparison of dynamics evolution between the analytic solution (left) and the numerical solution (right) for the first-order rogue wave solution under case (3) $\gamma_1 = 0$.

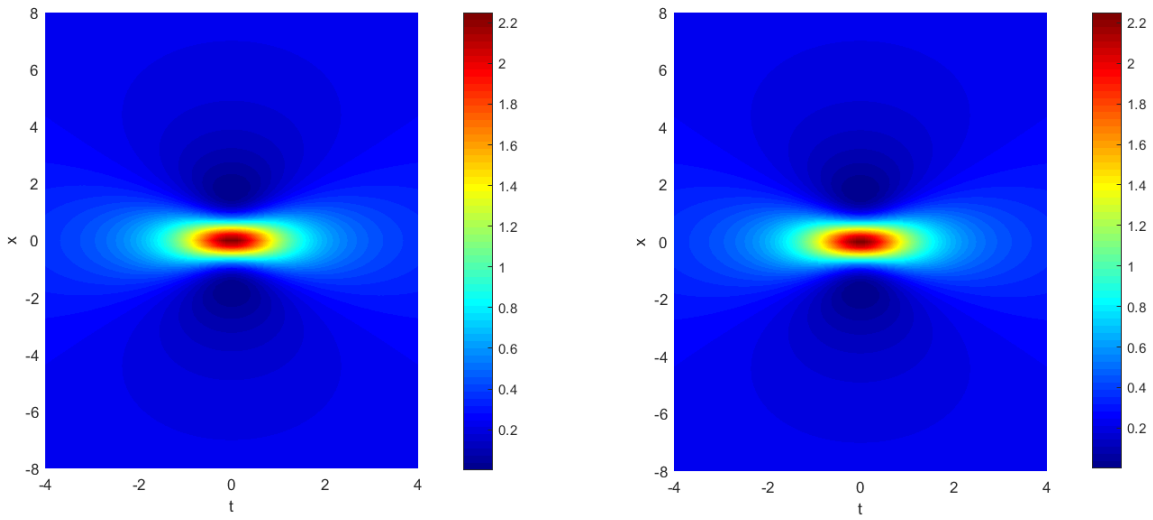

Figure 12. The planform between the analytic solution (left) and the numerical solution (right) of the first-order rogue wave solution under case (3) $\gamma_1 = 0$.

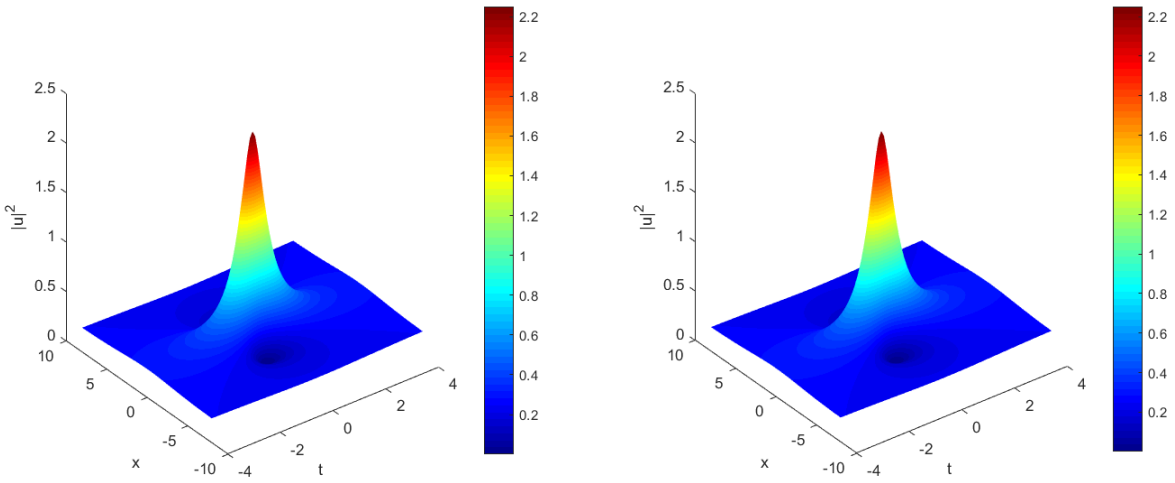

Figure 13. Comparison of dynamics evolution between the analytic solution (left) and the numerical solution (right) for the first-order rogue wave solution under case (4) $\gamma_1 = 0.5$.

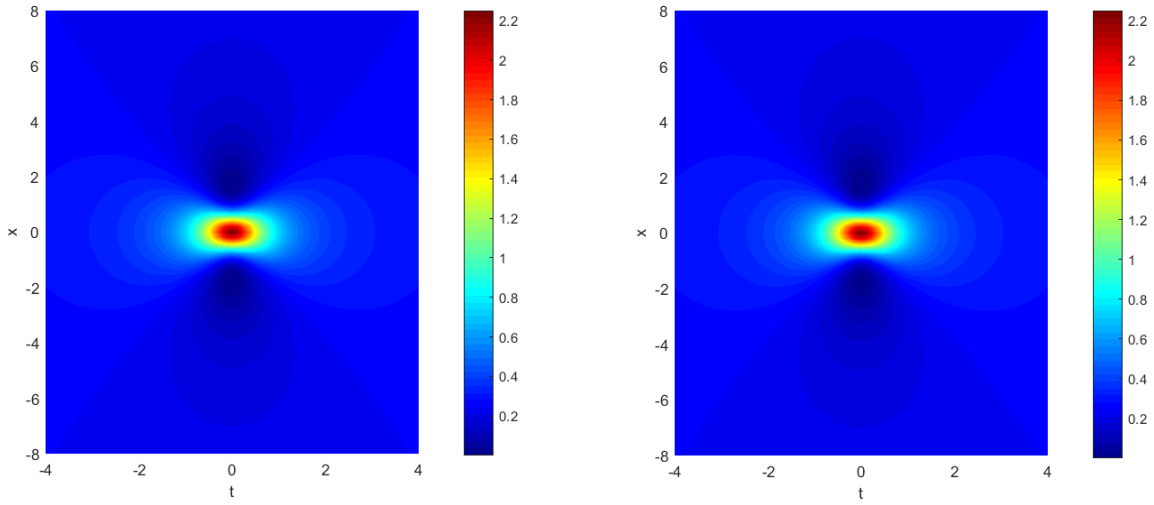

Figure 14. The planform between the analytic solution (left) and the numerical solution (right) of the first-order rogue wave solution under case (4) $\gamma_1 = 0.5$.

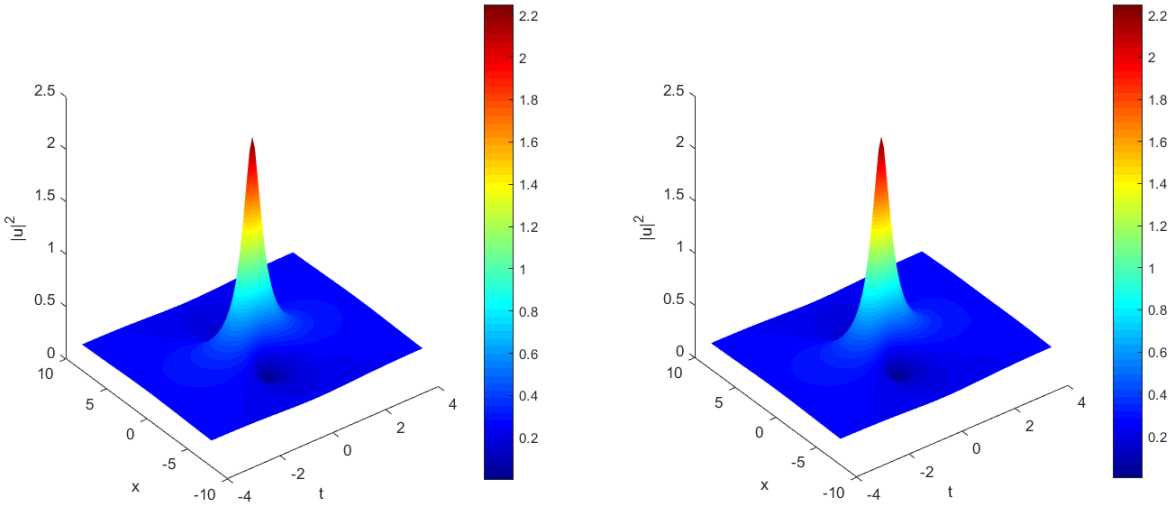

Figure 15. Comparison of dynamics evolution between the analytic solution (left) and the numerical solution (right) for the first-order rogue wave solution under case (5) $\gamma_1 = 1$.

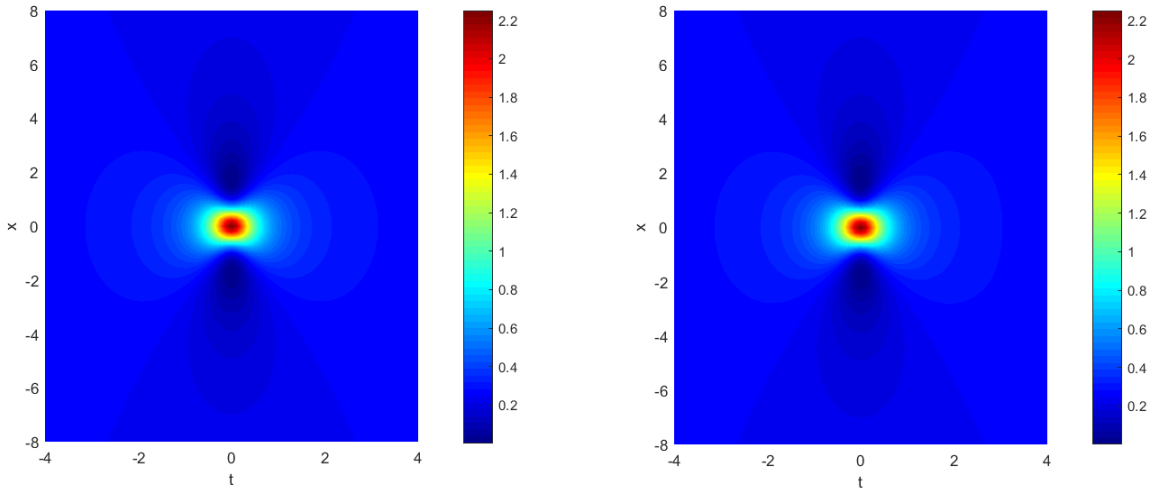

Figure 16. The planform between the analytic solution (left) and the numerical solution (right) of the first-order rogue wave solution under case (5) $\gamma_1 = 1$.

4. Conclusions and further questions

In conclusion, we have proposed three different finite difference schemes for GNLDS equation and we proved the conservation properties of the equation with periodic boundary condition. Moreover, the corresponding discrete conservation laws of the three schemes were advanced in discrete level. Among them, obviously CNFD-C scheme had better conservation properties. Furthermore, we gave

several typical numerical examples to confirm the corresponding convergence rates and conservation laws for the three schemes in discrete sense. In examples 3 and 4, we used CNFD-C scheme to simulate the collision of solitary waves and the first-order rogue wave solution. These numerical experiments verified the effectiveness of the proposed schemes.

However, the theoretical analysis of the schemes is a greater difficulty and challenge for us, which will be our further exploration direction in the future research process. We will also consider perfecting some work on the time fractional order of the generalized nonlinear Schrödinger equation, which is also a challenge for us in the future. In addition, it can be seen from the energy expression that the coefficient in front of the H^1 semi-norm of the solution of the original equation is negative, then in the case of energy conservation, the H^1 semi-norm cannot be controlled, and it may tend to infinity and the blow-up phenomenon may occur, and this article has not been optimized for this situation. Therefore, in the following work, readers can specifically optimize a format for blow-up phenomena.

Appendix A: The proof of conservation laws for problem (1.5)–(1.7).

Here, we give a brief proof of Lemma 1.1.

Proof. Make inner product of both sides of (1.5) with $u(x,t)$ at the same time, that is, multiply both sides of the equation by $\overline{u}(x,t)$, and integrate x from a to b. Then take the imaginary part of it, we get

$$\begin{aligned}&\frac{1}{2}\mathrm{Re}\int_a^b (u\overline{u})_t dx - \mathrm{Im}\int_a^b |u_x|^2 dx + 2\mathrm{Im}\int_a^b |u|^4 dx + \gamma_1 \mathrm{Im}\int_a^b |u_{xx}|^2 dx - 3\gamma_1 \mathrm{Im}\int_a^b |(u^2)_x|^2 dx \\ &- 2\gamma_1 \mathrm{Im}\int_a^b ((|u|^2)_x)^2 dx + 6\gamma_1 \mathrm{Im}\int_a^b |u|^6 dx = 0,\end{aligned} \tag{4.1}$$

$\mathrm{Re}(v)$ and $\mathrm{Im}(v)$ mean taking the real part and imaginary part of v respectively, we can get $\frac{d}{dt}Q(t) = 0$, where

$$Q(t) = \frac{1}{2}\int_a^b |u|^2 dx. \tag{4.2}$$

Then (1.8) holds. Likewise, make inner product of both sides of (1.5) with $u_t(x,t)$ at the same time, and then take the real part of both sides of (1.5), we can get

$$\begin{aligned}&\mathrm{Im}\int_a^b |u_t|^2 dx - \mathrm{Re}\int_a^b \overline{u}_t u_{xx} dx + 2\mathrm{Re}\int_a^b \overline{u}_t |u|^2 u dx + \gamma_1 \mathrm{Re}\int_a^b \overline{u}_t u_{xxxx} dx \\ &- 3\gamma_1 \mathrm{Re}\int_a^b \overline{u}_t (u^2)_{xx}\overline{u} dx + 2\gamma_1 \mathrm{Re}\int_a^b \overline{u}_t (u\overline{u})_{xx} u dx + 6\gamma_1 \mathrm{Re}\int_a^b \overline{u}_t |u|^4 u dx = 0.\end{aligned} \tag{4.3}$$

Due to the periodic boundary conditions, we get

$$\mathrm{Re}\int_a^b \overline{u}_t u_{xx} dx = \mathrm{Re}(\overline{u}_t u_x|_a^b - \int_a^b \overline{u}_{tx} u_x dx) = -\frac{1}{2}(\int_a^b \overline{u}_{tx} u_x + u_{tx}\overline{u}_x dx) = -\frac{1}{2}\int_a^b \frac{\partial}{\partial t}(u_x \overline{u}_x) dx,$$

the last five items of (4.3) are calculated similarly, so we obtain

$$\begin{aligned}
&\mathrm{Im}\int_a^b |u_t|^2dx - \frac{1}{2}\int_a^b \frac{\partial}{\partial t}(u_x\overline{u}_x)dx + \int_a^b |u|^2\frac{\partial}{\partial t}|u|^2dx + \frac{\gamma_1}{2}\int_a^b (u_{xx}\overline{u}_{txx} + u_{txx}\overline{u}_{xx})dx\\
&- 3\gamma_1\int_a^b |u_x|^2(|u|^2)_t + |u|^2(|u_x|^2)_t dx - \gamma_1\int_a^b (|u|^2)_x(u\overline{u}_t + u_t\overline{u})_x dx + 3\gamma_1\int_a^b |u|^4(u\overline{u}_t + u_t\overline{u})dx\\
=&-\frac{1}{2}\frac{d}{dt}\int_a^b |u_x|^2dx + \frac{1}{2}\frac{d}{dt}\int_a^b (|u|^2)^2dx + \frac{\gamma_1}{2}\frac{d}{dt}\int_a^b |u_{xx}|^2dx - 3\gamma_1\frac{d}{dt}\int_a^b |u_x|^2|u|^2dx\\
&-\frac{\gamma_1}{2}\frac{d}{dt}\int_a^b ((|u|^2)_x)^2dx + \gamma_1\frac{d}{dt}\int_a^b |u|^6dx\\
=&0,
\end{aligned}$$

we can get $\frac{d}{dt}E(t) = 0$, where

$$\begin{aligned}
E(t) =& -\frac{1}{2}\int_a^b |u_x|^2dx + \frac{1}{2}\int_a^b |u|^4dx + \frac{\gamma_1}{2}\int_a^b |u_{xx}|^2dx\\
&- 3\gamma_1\int_a^b |u_x|^2|u|^2dx - \frac{\gamma_1}{2}((|u|^2)_x)^2dx + \gamma_1\int_a^b |u|^6dx.
\end{aligned} \tag{4.4}$$

This implies (1.9) holds. Therefore we complete the proof of Lemma 1.1.

Appendix B: The proof of conservation laws for three schemes in discrete sense.

Here, we give the proof of Theorem 2.3 because the proof processes of Theorems 2.1–2.2 are similar to Theorem 2.3, so we only give the proof ideas for Theorems 2.1–2.2 and omit the processes of them.

Proof. Make the inner product of (2.7) and $(u^{n+1} + u^{n-1})$ and take the imaginary part of the equation to get

$$\begin{aligned}
&\frac{h}{2\tau}\sum_{j=0}^{J-1}(|u_j^{n+1}|^2 - |u_j^{n-1}|^2) - \frac{1}{2}\mathrm{Im}\sum_{j=0}^{J-1}|\delta_x^+(u_j^{n+1} + u_j^{n-1})|^2 + h\mathrm{Im}\sum_{j=0}^{J-1}|u_j^n|^2|u_j^{n+1} + u_j^{n-1}|^2\\
&+ \frac{h\gamma_1}{2}\mathrm{Im}\sum_{j=0}^{J-1}|\delta_x^2(u_j^{n+1} + u_j^{n-1})|^2 - \frac{3h\gamma_1}{2}\mathrm{Im}\sum_{j=0}^{J-1}|\delta_x^+(u_j^n(u_j^{n+1} + u_j^{n-1}))|^2\\
&- \frac{h\gamma_1}{2}\mathrm{Im}\sum_{j=0}^{J-1}(\delta_x^+(|u_j^{n+1}|^2 + |u_j^{n-1}|^2))^2 + h\gamma_1\mathrm{Im}\sum_{j=0}^{J-1}(|u_j^{n+1}|^6 + 2|u_j^{n+1}|^4|u_j^{n-1}|^2 + 2|u_j^{n-1}|^4|u_j^{n+1}|^2 + |u_j^{n-1}|^6)\\
=&\frac{h}{2\tau}\sum_{j=0}^{J-1}(|u_j^{n+1}|^2 - |u_j^{n-1}|^2)\\
=&0,
\end{aligned}$$

we can get $Q^n = Q^{n-1} = \cdots = Q^0$, where

$$Q^n = \frac{h}{2}\sum_{j=0}^{J-1}(|u_j^{n+1}|^2 + |u_j^n|^2). \tag{4.1}$$

Next, make the discrete inner product of (2.7) and $\delta_t u^n$, and then take the real part, we obtain

$$\begin{aligned}
&h\mathrm{Im}\sum_{j=0}^{J-1}|\delta_t u_j^n|^2-\frac{h}{4\tau}\sum_{j=0}^{J-1}(|\delta_x^+u_j^{n+1}|^2-|\delta_x^+u_j^{n-1}|^2)+\frac{h}{2\tau}\sum_{j=0}^{J-1}(|u_j^n|^2(|u_j^{n+1}|^2-|u_j^{n-1}|^2))\\
&+\frac{h\gamma_1}{4\tau}\sum_{j=0}^{J-1}(|\delta_x^2u_j^{n+1}|^2-|\delta_x^2u_j^{n-1}|^2)-\frac{3h\gamma_1}{4\tau}\sum_{j=0}^{J-1}(|\delta_x^+(u_j^nu_j^{n+1})|^2-|\delta_x^+(u_j^nu_j^{n-1})|^2)\\
&-\frac{h\gamma_1}{4\tau}\sum_{j=0}^{J-1}((\delta_x^+|u_j^{n+1}|^2)^2-(\delta_x^+|u_j^{n-1}|^2)^2)+\frac{h\gamma_1}{2\tau}\sum_{j=0}^{J-1}(|u_j^{n+1}|^6-|u_j^{n-1}|^6)\\
=&0,
\end{aligned}$$

we can get $E^n = E^{n-1} = \cdots = E^0$, where

$$\begin{aligned}
E^n=&-\frac{h}{4}\sum_{j=0}^{J-1}(|\delta_x^+u_j^{n+1}|^2+|\delta_x^+u_j^n|^2)+\frac{h}{2}\sum_{j=0}^{J-1}|u_j^n|^2|u_j^{n+1}|^2+\frac{h\gamma_1}{4}\sum_{j=0}^{J-1}(|\delta_x^2u_j^{n+1}|^2+|\delta_x^2u_j^n|^2)\\
&-\frac{3h\gamma_1}{4}\sum_{j=0}^{J-1}|\delta_x^+(u_j^nu_j^{n+1})|^2-\frac{h\gamma_1}{4}\sum_{j=0}^{J-1}((\delta_x^+|u_j^{n+1}|^2)^2+(\delta_x^+|u_j^n|^2)^2)+\frac{h\gamma_1}{2}\sum_{j=0}^{J-1}(|u_j^{n+1}|^6+|u_j^n|^6).
\end{aligned}\tag{4.2}$$

Therefore Theorem 2.3 holds.

Proof. We make the discrete inner product of (2.1) and $u^{n+\frac{1}{2}}$, and then take the imaginary part, therefore Theorem 2.1 holds.

Proof. We make the discrete inner product of (2.4) and $\delta_t^+u^n$, and then take the real part, therefore Theorem 2.2 holds.

Conflict of interest

There are no conflicts of interest to declare.

References

1. M. Lakshmanan, K. Porsezian, M. Daniel, Effect of discreteness on the continuum limit of the Heisenberg spin chain, *Phys. Lett. A.*, **133** (1988), 483–488. https://doi.org/10.1016/0375-9601(88)90520-8
2. L. H. Wang, K. Porsezian, J. S. He, Breather and rogue wave solutions of a generalized nonlinear Schrödinger equation, *Phys. Rev. E.*, **87** (2013), 053202. https://doi.org/10.1103/PhysRevE.87.053202
3. X. Zhang, Y. Chen, Inverse scattering transformation for generalized nonlinear Schrödinger equation, *Appl. Math. Lett.* , **98** (2019), 306–313. https://doi.org/10.1016/j.aml.2019.06.014
4. Z. Zhao, L. He, Resonance-type soliton and hybrid solutions of a (2+1)-dimensional asymmetrical Nizhnik-Novikov-Veselov equation, *Appl. Math. Lett.*, **122** (2021), 107497. https://doi.org/10.1016/j.aml.2021.107497

5. Z. Zhao, L. He, Nonlinear superposition between lump waves and other waves of the (2+1)-dimensional asymmetrical Nizhnik-Novikov-Veselov equation, *Nonlinear Dyn.*, **102** (2021), 555–568. https://doi.org/10.1007/s11071-022-07215-x
6. Z. Zhao, L. He, Lie symmetry, nonlocal symmetry analysis, and interaction of solutions of a (2+1)-dimensional KdV-mKdV equation, *Theor. Math. Phys.*, **206** (2021), 142–162. https://doi.org/10.1134/S0040577921020033
7. M. Jeli, B. Samet, C. Vetro, Nonexistence of solutions to higher order evolution inequalities with nonlocal source term on Riemannian manifolds, *Complex. Var. Elliptic.*, (2022) 1–18. https://doi.org/10.1080/17476933.2022.2061474
8. M. Jeli, B. Samet, C. Vetro, On the critical behavior for inhomogeneous wave inequalities with Hardy potential in an exterior domain, *Adv. Nonlinear Anal.*, **10** (2021), 1267–1283. https://doi.org/10.1515/anona-2020-0181
9. Q. Chang, E. Jia, W. Sun, Difference schemes for solving the generalized nonlinear equation, *J. Comput. Phys.*, **148** (1999), 397–415. https://doi.org/10.1006/jcph.1998.6120
10. M. Dehghan, A. Taleei, A compact split-step finite difference method for solving the nonlinear Schrödinger equations with constant and variable coefficients, *Comput. Phys. Commun.*, **181** (2010), 43–51. https://doi.org/10.1016/j.cpc.2009.08.015
11. Z. Gao, S. Xie, Fourth-order alternating direction implicit compact finite difference schemes for two-dimensional Schrödinger equations, *Appl. Numer. Math.*, **61** (2011), 593–614. https://doi.org/10.1016/j.apnum.2010.12.004
12. S. K. Lele, Compact finite difference schemes with spectral-like resolution, *J. Comput. Phys.*, **103** (1992), 16–42. https://doi.org/10.1016/0021-9991(92)90324-R
13. M. Subasi, On the finite difference schemes for the numerical solution of two dimensional Schrödinger equation, *Numer. Meth. Part. D. E.*, **18** (2002), 752–758. https://doi.org/10.1002/num.10029
14. T. Wang, B. Guo, Unconditional convergence of two conservative compact difference schemes for non-linear Schrödinger equation in one dimension, *Sci. Sin. Math.*, **41** (2011), 207–233. https://doi.org/10.1360/012010-846
15. T. Wang, X. Zhao, Unconditional L^∞ convergence of two compact conservative finite difference schemes for the nonlinear Schrödinger equation in multi-dimensions, *Calcolo*, **34** (2018). https://doi.org/10.1007/s10092-018-0277-0
16. T. Wang, B. Guo, Q. Xu, Fourth-order compact and energy conservative difference schemes for the nonlinear Schrödinger equation in two dimensions, *J. Comput. Phys.*, **243** (2013), 382–399. https://doi.org/10.1016/j.jcp.2013.03.007
17. T. Wang, B. Guo, L. Zhang, New conservative difference schemes for a coupled nonlinear Schrödinger system, *Appl. Math. Comput.*, **217** (2010), 1604–1619. https://doi.org/10.1016/j.amc.2009.07.040
18. T. Wang, T. Nie, L. Zhang, F. Chen, Numerical simulation of a nonlinearly coupled Schrödinger system: A linearly uncoupled finite difference scheme, *Math. Comput. Simulat.*, **79** (2008), 607–621. https://doi.org/10.1016/j.matcom.2008.03.017

19. T. Wang, A linearized, decoupled, and energy-preserving compact finite difference scheme for the coupled nonlinear Schrödinger equations, *Numer. Meth. Part. D. E.*, **33** (2017), 840–867. https://doi.org/10.1002/num.22125

20. T. Wang, L. Zhang, Analysis of some new conservative schemes for nonlinear Schrödinger equation with wave operator, *Appl. Math. Comput.*, **182** (2006), 1780–1794. https://doi.org/10.1016/j.amc.2006.06.015

21. S. Xie, G. Li, S. Yi, Compact finite difference schemes with high accuracy for one-dimensional nonlinear Schrödinger equation, *Comput. Method. Appl. M.*, **198** (2009), 1052–1060. https://doi.org/10.1016/j.cma.2008.11.011

22. Z. Fei, V. M. Pérez-Grarcíz, L. Vázquez, Numerical simulation of nonlinear Schrödinger systems: a new conservative scheme, *Appl. Math. Comput.*, **71** (1995), 165–177. https://doi.org/10.1016/0096-3003(94)00152-T

23. Q. Chang, E. Jia, W. Sun, Difference schemes for solving the generalized nonlinear Schrödinger equation, *J. Comput. Phys.*, **148** (1999), 397–415. https://doi.org/10.1006/jcph.1998.6120

24. J. Argyris, M. Haase, An engineer's guide to solitons phenomena: application of the finite element method, *Comput. Method. Appl. M.*, **61** (1987), 71–122. https://doi.org/10.1016/0045-7825(87)90117-4

25. G. Akrivis, V. Dougalis, O. Karakashian, On fully discrete Galerkin methods of second-order temporal accuracy for the nonlinear Schrödinger equation, *Numer. Math.*, **59** (1991), 31–53. https://doi.org/10.1007/BF01385769

26. L. R. T. Gardner, G. A. Gardner, S. I. Zaki, Z. El Sahrawi, B-spline finite element studies of the non-linear Schrödinger equation, *Comput. Method. Appl. M.*, **108** (1993), 303–318. https://doi.org/10.1016/0045-7825(93)90007-K

27. O. Karakashian, C. Makridakis, A space-time finite element method for the nonlinear Schrödinger equation: the discontinuous Galerkin method, *Math. Comput.*, **67** (1998), 479–499. https://doi.org/10.1090/S0025-5718-98-00946-6

28. Y. Xu, C. W. Shu, Local discontinuous Galerkin methods for nonlinear Schrödinger equations, *J. Comput. Phys.*, **205** (2005), 72–77. https://doi.org/10.1016/j.jcp.2004.11.001

29. M. Dehghan, D. Mirzaei, Numerical solution to the unsteady two-dimensional Schrödinger equation using meshless local boundary integral equation method, *Int. J. Numer. Meth. Eng.*, **76** (2008), 501–520. https://doi.org/10.1002/nme.2338

30. M. Dehghan, D. Mirzaei, The meshless local Petrov-Galerkin (MLPG) method for the generalized two-dimensional non-linear Schrödinger equation, *Eng. Anal. Bound. Elem.*, **32** (2008), 747–756. https://doi.org/10.1016/j.enganabound.2007.11.005

31. B. M. Caradoc-Davis, R. J. Ballagh, K. Burnett, Coherent dynamics of vortex formation in trapped Bose-Einstein condensates, *Phys. Rev. Lett.*, **83** (1999), 895–898. https://doi.org/10.1103/PhysRevLett.83.895

32. M. Dehghan, A. Taleei, Numerical solution of nonlinear Schrödinger equation by using time-space pseudo-spectral method, *Numer. Meth. Part. D. E.*, **26** (2010), 979–992. https://doi.org/10.1002/num.20468

33. D. Pathria, J. L. Morris, Pseudo-spectral solution of nonlinear Schrödinger equations, *J. Comput. Phys.*, **87** (1990), 108–125. https://doi.org/10.1016/0021-9991(90)90228-S

34. W. Bao, D. Jaksch, P. A. Markowich, Numerical solution of the Gross-Pitaevskii equation for Bose-Einstein condensation, *J. Comput. Phys.*, **187** (2003), 318–342. https://doi.org/10.1016/S0021-9991(03)00102-5

35. W. Bao, H. Li, J. Shen, A generalized-Laguerre-Fourier-Hermite pseudospectral method for computing the dynamics of rotating Bose-Einstein condensates, *Siam. J. Sci. Comput.*, **31** (2009), 3685–3711. https://doi.org/10.1137/080739811

36. W. Bao, J. Shen, A fourth-order time-splitting Laguerre-Hermite pseudo-spectral method for Bose-Einstein condensates, *Siam. J. Sci. Comput.*, **26** (2005), 2010–2028. https://doi.org/10.1137/030601211

37. M. Thalhammer, High-Order Exponential Operator Splitting Methods for Time-Dependent Schrödinger Equations, *SIAM.*, **46** (2008), 2022–2038. https://doi.org/10.1137/060674636

38. X. Antoine, C. Besse, V. Rispoli, High-order IMEX-spectral schemes for computing the dynamics of systems of nonlinear Schrödinger/Gross-Pitaevskii equations, *J. Comput. Phys.*, **327** (2016), 252–269. https://doi.org/10.1016/j.jcp.2016.09.020

39. Y. Gong, Q. Wang, Y. Wang, J. Cai, A conservative Fourier pseudo-spectral method for the nonlinear Schrödinger equation, *J. Comput. Phys.*, **328** (2017), 354–370. https://doi.org/10.1016/j.jcp.2016.10.022

40. R. Zhang, J. Zhu, X. Yu, M. Li, A. F. D. Loula, A conservative spectral collocation method for the nonlinear Schrödinger equation in two dimensions, *Appl. Math. Comput.*, **310** (2017), 194–203. https://doi.org/10.1016/j.amc.2017.04.035

41. T. Wang, J. Wang, B. Guo, Two completely explicit and unconditionally convergent Fourier pseudo-spectral methods for solving the nonlinear Schrödinger equation, *J. Comput. Phys.*, **404** (2020), 109116. https://doi.org/10.1016/j.jcp.2019.109116

42. S. Wang, T. Wang, L. Zhang, Numerical computations for N-coupled nonlinear Schrödinger equations by split step spectral methods, *Appl. Math. Comput.*, **222** (2013), 438–452. https://doi.org/10.1016/j.amc.2013.07.060

43. M. Li, J. Zhao, N. Wang, S. Chen, Conforming and nonconforming conservative virtual element methods for nonlinear Schrödinger equation: A unified framework, *Comput. Method. Appl. M.*, **380** (2021), 113793. https://doi.org/10.1016/j.cma.2021.113793

44. M. Li, Y. Zhao, A fast energy conserving finite element method for the nonlinear fractional Schrödinger equation with wave operator, *Appl. Math. Comput.*, **338** (2018), 758–773. https://doi.org/10.1016/j.amc.2018.06.010

45. L. Wang, M. Li, Galerkin finite element method for damped nonlinear Schrödinger equation, *Appl. Numer. Math.*, **178** (2022), 216–247. https://doi.org/10.1016/j.apnum.2022.03.018

46. X. He, X. Lü, M-lump solution, soliton solution and rational solution to a (3+1)-dimensional nonlinear model, *Math. Comput. Simulat.*, **197** (2022), 327–340. https://doi.org/10.1016/j.matcom.2022.02.014

47. X. Lü, S. Chen, Interaction solutions to nonlinear partial differential equations via Hirota bilinear forms: one-lump-multi-stripe and one-lump-multi-soliton types, *Nonlinear Dyn.*, **103** (2021), 947–977. https://doi.org/10.1007/s11071-020-06068-6

48. P. Debnath, N. Konwar, S. Radenovic, *Metric Fixed Point Theory: Applications in Science, Engineering and Behavioural Sciences*, Springer Singapore, 2021. https://doi.org/10.1007/978-981-16-4896-0

49. V. Todorcevi, *Harmonic Quasiconformal Mappings and Hyperbolic Type Metrics*, Springer Cham, 2019. https://doi.org/10.1007/978-3-030-22591-9

50. V. Todorcevi, Subharmonic behavior and quasiconformal mappings, *Anal. Math. Phys.*, **9** (2019), 1211–1225. https://doi.org/10.1007/s13324-019-00308-8

51. N. Fabiano, S. Radenovi, On scaling of Schrödinger equation and some results for heavy quarks mesons, *Nat. Sci.*, **11** (2021), 49–53. https://doi.org/10.5937/bnsr11-31433

52. W. Bao, S. Jin, P. A. Markowich, On time-splitting spectral approximation for the Schrödinger equation in the semiclassical regime, *J. Comput. Phys.*, **175** (2002), 487–524. https://doi.org/10.1006/jcph.2001.6956

53. P. A. Markowich, P. Pietra, C. Pohl, Numerical approximation of quadratic observables of Schrödinger-type equations in the semi-classical limit, *Numer. Math.*, **81** (1999), 595–630. https://doi.org/10.1007/s002110050406

54. M. Thalhammer, M. Caliari, C. Neuhauser, High-order time-splitting Hermite and Fourier spectral methods, *J. Comput. Phys.*, **228** (2009), 822–832. https://doi.org/10.1016/j.jcp.2008.10.008

AIMS Press